

GeAs: Highly anisotropic van der Waals thermoelectric material

Kathleen Lee, Saeed Kamali, Tore Ericsson, Maverick Bellard, and Kirill Kovnir

Chem. Mater., **Just Accepted Manuscript** • DOI: 10.1021/acs.chemmater.6b00567 • Publication Date (Web): 18 Mar 2016

Downloaded from <http://pubs.acs.org> on March 22, 2016

Just Accepted

“Just Accepted” manuscripts have been peer-reviewed and accepted for publication. They are posted online prior to technical editing, formatting for publication and author proofing. The American Chemical Society provides “Just Accepted” as a free service to the research community to expedite the dissemination of scientific material as soon as possible after acceptance. “Just Accepted” manuscripts appear in full in PDF format accompanied by an HTML abstract. “Just Accepted” manuscripts have been fully peer reviewed, but should not be considered the official version of record. They are accessible to all readers and citable by the Digital Object Identifier (DOI®). “Just Accepted” is an optional service offered to authors. Therefore, the “Just Accepted” Web site may not include all articles that will be published in the journal. After a manuscript is technically edited and formatted, it will be removed from the “Just Accepted” Web site and published as an ASAP article. Note that technical editing may introduce minor changes to the manuscript text and/or graphics which could affect content, and all legal disclaimers and ethical guidelines that apply to the journal pertain. ACS cannot be held responsible for errors or consequences arising from the use of information contained in these “Just Accepted” manuscripts.

GeAs: Highly anisotropic van der Waals thermoelectric material

Kathleen Lee,[§] Saeed Kamali,[#] Tore Ericsson,[&] Maverick Bellard,[§] Kirill Kovnir^{§,*}

[§]Department of Chemistry, University of California, Davis, One Shields Avenue, Davis, CA 95616

[#]Mechanical, Aerospace & Biomedical Engineering Department, University of Tennessee Space Institute, Tullahoma, TN 37388

[&]Department of Chemistry, Ångström Laboratory, Uppsala University, Box 538, SE-75121 Uppsala, Sweden

Layered Arsenide, crystal structure, anisotropy, thermoelectric

ABSTRACT: GeAs and Sn-doped GeAs were synthesized from elements. Both crystallize in a layered crystal structure in the $C2/m$ space group (No. 12) in the GaTe structure type. The crystal structure consists of As-terminated layers separated by van der Waals gaps. ¹¹⁹Sn Mössbauer spectroscopy reveals that in the doped compound, Sn atoms are situated in a symmetric and homogeneous environment, most probably in the form of Sn₂ dumbbells. The anisotropic crystal structure of GeAs leads to highly anisotropic electronic and thermal transport properties. High electrical and thermal conductivities were determined along the crystallographic layers. For the perpendicular direction across the layers, a sharp drop of more than an order of magnitude was observed for the transport properties of the GeAs single crystal. As a result, an order of magnitude difference in the figure of merit, ZT , was achieved. High-temperature thermoelectric characterization of the Sn-doped compound reveals a remarkable ZT with a maximum of 0.35 at 660 K.

INTRODUCTION Efficient thermoelectric materials are highly sought after for use in space applications, such as in the Mars Rover, Curiosity. Thermoelectric materials also have potential domestic applications in thermoelectric cooling and waste heat recovery. The efficiency of thermoelectric materials is determined from the dimensionless figure of merit, ZT , defined as $ZT = S^2T/\kappa\rho$, where S is the Seebeck coefficient or thermopower, T is temperature, κ is the thermal conductivity, and ρ is the electrical resistivity. Efficient thermoelectric materials exhibit high thermopower, low thermal conductivity, and high electrical conductivity. To optimize ZT , often complex and large crystal structures are sought after to reduce the thermal conductivity. Another approach to reduce thermal conductivity is to utilize the phonon glass-electron crystal (PGEC) concept¹ where the compound possesses a well-defined crystal structure to provide good electrical conductivity with weakly bonded atoms or fragments to scatter phonons, as in a glass. Inorganic clathrates are typical PGEC systems since they are composed of 3D frameworks that effectively conduct electrons with guest atoms encapsulated in large cages that are capable of rattling to scatter phonons.²⁻⁴ Similarly, Sb- and Bi-based Zintl phases have anionic frameworks that serve as the electron crystal with complex structural features that scatter phonons.⁵⁻⁸

Anisotropy of the crystal structure adds one more level of complexity. Anisotropic crystal structures, such as van der Waals solids, have recently gained attention due to

anharmonicity leading to low thermal conductivities and high figures of merit.⁹⁻¹² SnSe, a layered material, was shown to have an unprecedentedly high figure of merit of 2.6 along one crystallographic direction.¹³ Moreover, the compound was shown to have strongly anisotropic transport properties along different crystallographic directions. Anisotropic properties are not commonly reported for layered materials since this requires growth of relatively large single crystals. Nevertheless, the anisotropic transport properties are important for understanding the structure-properties correlations in thermoelectric materials. Germanium arsenide belongs to an underexplored family of binary van der Waals compounds formed from tetrel (group 14) and pnictogen (group 15) elements. Herein, we discuss the synthesis and crystal structure of GeAs, doping with Sn, and the anisotropic thermal and electronic transport properties that stem from the crystal structure.

EXPERIMENTAL

Warning: At high temperatures the As vapor pressure may be sufficient to damage the reaction ampoules, which may result in an explosion releasing toxic As vapor. The concentration of As should be kept to a minimum.

SYNTHESIS The starting materials, Ge (Alfa Aesar, 99.999%), As (Alfa Aesar, 99.9999%), and Sn shot (Alfa Aesar, 99.7) were used as received. GeAs was synthesized by combining a stoichiometric amount of Ge with a 3-5 wt% excess of As leading to Ge:As ratios of 1:1.03-1.05. The

elements (total mass < 1 g) were sealed inside evacuated silica ampoules. The ampoules were heated to 1373 K over 48 hours, annealed at this temperature for 4-5 days, and then cooled inside the furnace. GeAs forms from a melt, so the product is a single ingot. Excess As was removed from the sample by sublimation in a sealed silica ampoule in a temperature gradient of 300/773 K with the sample placed in the hot temperature zone.

Sn-doped GeAs was synthesized using a flux method by combining Sn:Ge:As in a 2:1:2 molar ratio inside sealed and evacuated silica ampoules. The same heating profile as pure GeAs was used. After annealing, the samples were prepared for centrifugation and excess Sn and Sn₄As₃ were removed by centrifuging at 873 K. The final products were washed with a 1:1 HCl:H₂O solution for several hours to remove any remaining amounts of Sn and Sn₄As₃. The Sn content was determined by energy dispersive X-ray (EDX) spectroscopy. Compounds with smaller amounts of Sn-doping were prepared by combining the elements in the desired ratio, e.g., 3% Sn-doped samples were prepared by combining the elements in a 0.03 Sn : 0.97 Ge : 1.00 As ratio and annealed at the same conditions as above. The products were checked for purity by powder X-ray diffraction and no further treatment was found to be necessary (Figure S1).

DIFFERENTIAL SCANNING CALORIMETRY (DSC) GeAs and Sn-doped GeAs were analyzed with a Netzsch Differential Scanning Calorimeter. DSC measurements were performed on ~30 mg of sample sealed inside evacuated silica ampoules. The samples were heated to 1273 K and cooled to 373 K with a heating/cooling rate of 10 K/min.

X-RAY DIFFRACTION Powder X-ray diffraction (XRD) was performed on a Rigaku 600 Miniflex employing Cu-K_α radiation with a Ni-K_β filter. Room temperature unit cell parameters were calculated using NIST LaB₆ SRM660c as a standard. Single crystal XRD was performed on a Bruker AXS SMART diffractometer employing Mo-K_α radiation with an APEX-II CCD detector. The datasets were collected at 90 K and recorded as ω-scans with a 0.3° step width. The datasets were integrated using the Bruker SAINT software and multiscan absorption corrections were applied. The solutions and refinements were performed using the SHELX suite.¹⁴ The structures of GeAs and Sn-doped GeAs were solved in the monoclinic space group, C₂/m. A summary of pertinent information relating to the unit cell parameters, data collection, and refinement is provided in Table 1 and the atomic parameters and interatomic distances are provided in Tables S1 and S2. Details of the crystal structure determination of the Sn-doped sample are discussed in the Results and Discussion section.

SCANNING ELECTRON MICROSCOPY Elemental analyses of selected single crystals of GeAs, Sn-doped GeAs, and their respective sintered pellets were performed on a Hitachi S4100T scanning electron microscope (SEM) with EDX (Oxford INCA Energy).

QUANTUM CHEMICAL CALCULATIONS Electronic structure calculations and bonding analyses for GeAs were carried out using the tight binding-linear muffin tin orbitals-atomic sphere approximation (TB-LMTO-ASA) program.¹⁵⁻¹⁹ The Barth-Hedin exchange potential was employed for the LDA calculations.¹⁶ The radial scalar-relativistic Dirac equation was solved to obtain the partial waves. The basis set used contained Ge(4s,4p) and As(4s,4p) orbitals with downfolded Ge(4d) and As(4d) functions. The density of states and band structures were calculated after converging the total energy on a dense *k*-mesh of 24×24×26 points with 1272 irreducible *k*-points.

¹¹⁹Sn MÖSSBAUER SPECTROSCOPY ¹¹⁹Sn Mössbauer spectroscopy was performed at room temperature on an X2000 spectrometer operating in constant acceleration mode in transmission geometry. Measurements were performed with a Ca¹¹⁹SnO₃ source maintained at room temperature. Isomer chemical shifts are referenced to the Ca¹¹⁹SnO₃ absorber. The spectrum was least squares fitted using the Recoil software.²⁰ The parameters from the fittings include the isomer shift ($\delta = 1.68 \text{ mm}\cdot\text{s}^{-1}$), quadrupole splitting ($\Delta E_Q = 0.44 \text{ mm}\cdot\text{s}^{-1}$), linewidth ($\Gamma = 0.81 \text{ mm}\cdot\text{s}^{-1}$), and intensity ($I = 100\%$). All e.s.d. are smaller than 0.01 mm·s⁻¹.

Table 1. Data collection and structural refinement parameters for GeAs and Sn-doped GeAs.^a

Compound	GeAs	Sn _{0.08(2)} Ge _{0.92} As
Space Group	C ₂ /m (No. 12)	
Temperature [K]	90(2)	
λ [Å]	Mo-K _α : 0.71073	
<i>a</i> [Å]	15.618(3)	15.697(19)
<i>b</i> [Å]	3.7948(7)	3.810(5)
<i>c</i> [Å]	9.5127(17)	9.548(12)
β [Å]	101.115(2)	101.122(17)
<i>V</i> [Å ³]	553.20(17)	560.3(12)
<i>Z</i>	12	
ρ [g/cm ³]	5.31	5.38
μ [mm ⁻¹]	33.84	33.21
θ [degrees]	2.18 < θ < 30.6	2.64 < θ < 29.0
Data/param.	977/37	846/39
<i>R</i> ₁	0.027	0.046
<i>wR</i> ₂	0.063	0.113
Goodness-of-fit	1.06	1.03
Diff. peak/hole [e/Å ³]	1.75/-1.23	3.82/-1.90

^a Further details pertaining to the crystal structure determination may be obtained from the Inorganic Crystal Structure Database (ICSD) at Fachinformationszentrum Karlsruhe, Germany, by quoting the depository numbers 430819 (GeAs) and 430820 (Sn-doped GeAs).

SPARK PLASMA SINTERING High-density pellets were pressed for GeAs (5 mm Ø) and Sn_{0.03}Ge_{0.97}As (12.7 mm Ø). Samples were ground into fine powder and loaded into graphite dies between circles of graphite foil. Graphite plungers were used for the 12.7 mm diameter pellet, while tungsten carbide plungers were used for the 5 mm diameter pellet to withstand high pressures. The samples were sintered using a Dr. Sinter Lab Jr. SPS-211Lx (Sumitomo Coal Mining Co., Ltd.) 5 mm/12.7 mm diameter pellets were sintered by heating samples to 523 K over a period of 5 min under a uniaxial pressure of 51/8 MPa, then heated to 773 K over a period of 45 min at which point the pressure was increased to 158/87 MPa, and annealed at this temperature for 10 minutes. Afterwards, the pressure was released and the sample was allowed to cool to room temperature. Samples were removed from the graphite dies and polished to remove traces of the graphite foil. The relative densities of the pellets were measured using the Archimedes method and found to be 96% for the 5 mm GeAs pellet and 89% for the 12.7 mm Sn_{0.03}Ge_{0.97}As pellet.

TRANSPORT PROPERTIES Transport properties were measured for both an oriented crystal of GeAs (5.2x4.6x0.5 mm) and pellets of GeAs (5 mm Ø pellet) and Sn-doped GeAs (12.7 mm Ø pellet). The crystal was measured in the directions parallel to the layers and perpendicular to the layers.

Low temperature (< 400 K) resistivity measurements were performed using a standard 4-probe *ac* measurement to exclude the resistance of the leads on a commercial multipurpose Physical Properties Measurement System (PPMS, Quantum Design). The low temperature thermal conductivity and Seebeck coefficient were also measured on the PPMS using the Thermal Transport Option. High temperature (300-700 K) thermal diffusivity was measured on a Nietzsche LFA 457 using Pyroceram 9606 as a reference material. The thermal conductivity, κ , was calculated based on the thermal diffusivity and heat capacity of the material using the equation $\kappa = D \cdot C_p \cdot d$, where D is the thermal diffusivity, C_p is the heat capacity, and d is the density of the pellet. The high temperature resistivity and Seebeck coefficient were measured on a Linseis LSR-3.

RESULTS AND DISCUSSION

SYNTHESIS AND THERMAL STABILITY GeAs was first reported by *Stöhr and Klemm* in 1939²¹ and again by *Wadsten* in 1977.²² The reported structure was assumed based on the analogous structure of SiAs. Four years later, *Mentzen et al.* reported the crystal structure of GeAs from

a GeAs crystal grown from a melt.²³ The reported synthetic procedures did not yield bulk quantities of phase pure GeAs. Our first attempt to synthesize GeAs using a stoichiometric ratio of Ge and As resulted in the formation of GeAs samples contaminated with unreacted Ge and As. The addition of an extra amount (3-5 wt%) of As ensured the complete reaction of Ge. Any remaining unreacted As was removed from the samples by subliming the As. The product was a single ingot composed of black plate-like crystals. GeAs is stable against ambient conditions and is also stable against concentrated HCl.

The most tin-rich sample of Sn-doped GeAs was synthesized using a Sn flux from a combination of elements in a 2:1:2 ratio of Sn:Ge:As. The Sn-doped GeAs sample was centrifuged at 873 K to remove excess Sn or tin arsenides that may have formed. The samples were additionally washed in a 1:1 HCl:H₂O solution for several hours to dissolve any remaining tin or tin arsenide impurities. Sn-doped GeAs is not stable in concentrated HCl, with the slow leaching of Sn from the compound after several hours in the acid wash. The use of Sn flux produced samples with the highest Sn content (~8%). This is similar to the maximum substitution achieved for Sn-doped GeP.²⁴ Smaller doping contents can be achieved by using the appropriate stoichiometric ratios of elements without flux: $x\text{Sn} : (1-x)\text{Ge} : 1\text{As}$ for Sn_{*x*}Ge_{*1-x*}As, $x < 0.1$.

Differential scanning calorimetry of GeAs shows the onset of melting at 1018(2) K and the onset of crystallization at 1008(2) K (Figure S2). Sn-doped GeAs has a lower melting point, with an onset of 1006(2) K and a crystallization onset of 1006(2) K for the sample with a nominal 3% Sn doping. Unlike the related GeP and Sn-doped GeP²⁴ where the difference in melting temperatures were >200 K, Sn-doped GeAs and GeAs do not have as large of a difference in melting temperature. Previous reports state a higher equilibrium melting temperature for GeAs (1036 K).²⁵⁻²⁷ In these works the phase diagram was produced with measurements conducted in an apparatus with saturated As pressure while our experiments were conducted by placing solid GeAs inside sealed and evacuated ampoules. The lack of As in the gas phase below the melting point may affect the equilibrium by decreasing the melting temperature. Our conditions for thermal analysis are closer to the method used by *Stöhr and Klemm* who reported GeAs melting point as 1010 K which is much closer to our reported temperature.²¹

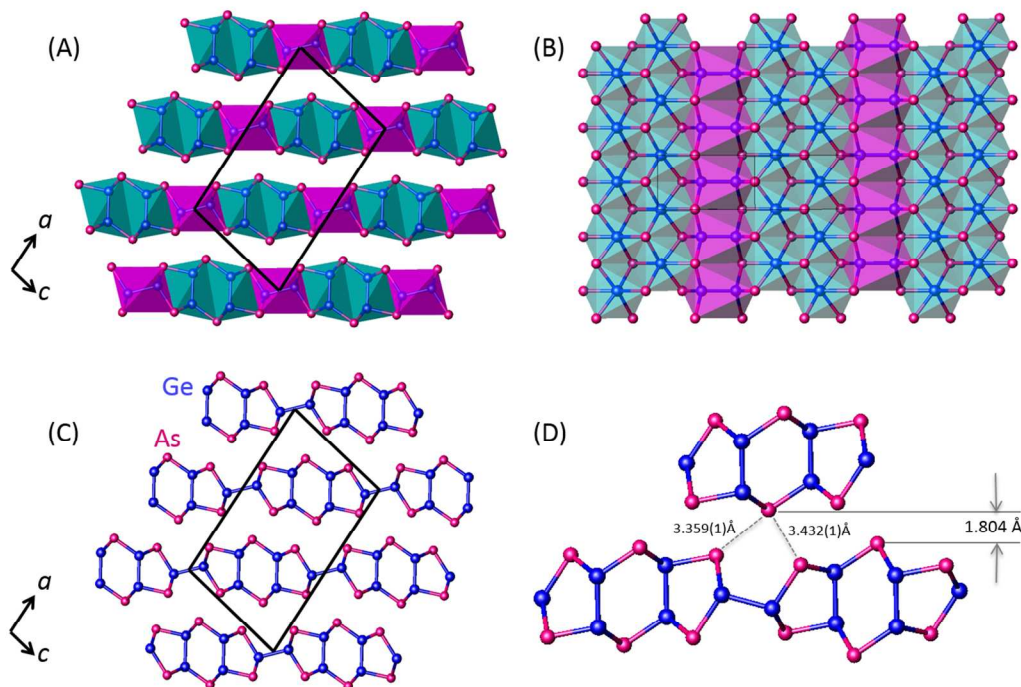


Figure 1. Crystal structure of GeAs. A. Polyhedral view; B. Top view of a single layer; C. Ball and stick model; D. Fragment of GeAs showing the shortest As-As distances and interlayer spacing. Ge: blue; As: red; $\text{Ge}_2@As_6$ polyhedra: blue and pink.

CRYSTAL STRUCTURE AND ^{119}Sn MÖSSBAUER SPECTROSCOPY GeAs is isostructural to other tetravalent pnictides such as GeP and SiAs, crystallizing in the GaTe structure type²⁸ in the space group $C2/m$ (No. 12). Similar to GeP, GeAs crystallizes in a layered structure. Within each layer Ge-Ge dumbbells are surrounded by a distorted trigonal antiprism of As atoms, as shown by the polyhedra in Figure 1. The layer is composed of edge-sharing polyhedra that are oriented orthogonal to each other and either parallel to or perpendicular to the layers (Figure 1). Two types of polyhedra rotated with respect to each other by 90° are emphasized: blue $\text{Ge}_2@As_6$ where the Ge_2 dumbbell is oriented perpendicular to the layers, and pink $\text{Ge}_2@As_6$ where the Ge_2 dumbbell is almost parallel to the layers (Figures 1A and 1B). Each layer is terminated by As atoms, with strong covalent bonding within the layers and van der Waals interactions across the layers. The shortest As-As distance is $3.359(1)$ Å and the interlayer spacing is 1.80 Å (Figures 1C and 1D). The structure reported by *Mentzen et al.*²³ had smaller unit cell parameters with a unit cell volume that is 10 Å³ smaller than the structure determined herein from the single crystal dataset collected at 90 K. Least square refinement of the room temperature powder diffraction data using LaB_6 as an internal standard resulted in the unit cell $a = 15.507(8)$ Å, $b = 3.776(2)$ Å, $c = 9.456(6)$ Å, $\beta = 101.04(2)$ Å. These unit cell parameters are identical within 2 e.s.d. to the unit cell reported by *Mentzen et al.*²³ and smaller than the unit cell parameters determined at 90 K (Table 1). More detailed variable temperature diffraction studies are necessary to clarify the possibility of thermal expansion of GeAs upon cooling.

Each Ge atom is coordinated by three As atoms and one Ge atom with Ge-As distances of 2.45 - 2.49 Å and Ge-Ge distances of 2.45 - 2.46 Å (Figure 1). While the Ge_3 - Ge_3 distance and the range of Ge-As distances reported by *Mentzen* are similar to this work, the Ge_1 - Ge_2 distance reported here is 0.02 Å larger than the previously reported structure.²³ The Ge-As distances are comparable to distances found in transition metal germanium arsenides (2.43 Å for ZnGeAs_2 and 2.46 Å for CdGeAs_2),²⁹ alkaline-earth germanium arsenides (2.42 Å for BaGe_2As_2 ,³⁰ 2.39 - 2.47 Å for $\text{Ca}_3\text{Ge}_2\text{As}_4$,³¹ 2.41 - 2.49 Å for $\text{Sr}_3\text{Ge}_2\text{As}_4$),³² and the clathrate $\text{Ge}_38\text{As}_8\text{I}_8$ (2.40 and 2.50 Å).³³

Similar to Sn-doped GeP, Sn-doping into GeAs causes significant disorder and split positions in the crystal structure. Refinement of the simple GeAs model for the Sn-doped compound resulted in high R -values and large anisotropic displacement parameters for all atoms. Moreover, all Ge positions exhibit occupancies $>100\%$. To achieve reasonable descriptions of the Sn/Ge positions, they were refined in isotropic mode. A high electron density peak was found near each Ge position and refined as Sn with the constraints that the total occupancy was 100% for those positions and the ADPs were equivalent. In the next cycles of refinement additional electron density peaks were found near each As atomic position. Those positions can be refined as either As or Ge with identical results since Ge and As are neighbors in the periodic system. Based on the results for the similar Sn-doped GeP we expect a certain amount of Ge in the As positions. For simplicity of description those positions were finally refined in anisotropic mode as As atoms only.

Analysis of interatomic distances indicates that the distances around the split position M1 cannot be described simply by two separate Sn and Ge positions. Proper distances and occupancies were achieved for the refinement of position M1 jointly occupied with Sn and Ge (grey atoms in Figure 2) and an additional Ge11 position in close proximity of position M1. The bottom part of Figure 2 represents the analysis of possible interatomic distances as well as atomic occupancies in the bimetallic dumbbells. Ge-Ge distances of 2.32 Å, 2.46 Å, and 2.54 Å are close to the distances in pristine GeAs, Ge-based inorganic clathrates and binary $R\text{Ge}_{2-x}$ phases, $R = \text{rare-earth metal}$.³⁴⁻³⁷ In turn, Sn-Sn distances are significantly longer, typically in the range of 2.75-2.9 Å.³⁸⁻⁴³

The resulting refined composition was $\text{Sn}_{0.08(2)}\text{Ge}_{0.92}\text{As}$. The composition obtained by EDX spectroscopy, $\text{Sn}_{0.04(2)}\text{Ge}_{1.00(2)}\text{As}_{0.96(2)}$, had a slight As deficiency compared to Ge (Figure S3). In order to maintain high Ge content, it is expected that Ge dopes slightly into the As site, assuming the composition of $[\text{Sn}_{0.04}\text{Ge}_{0.96}][\text{As}_{0.96}\text{Ge}_{0.04}]$. EDX spectroscopy of the sample with the nominal composition $\text{Sn}_{0.03}\text{Ge}_{0.97}\text{As}$ gave a composition of $[\text{Sn}_{0.03(1)}\text{Ge}_{0.97}][\text{As}_{0.98(1)}\text{Ge}_{0.02}]$.

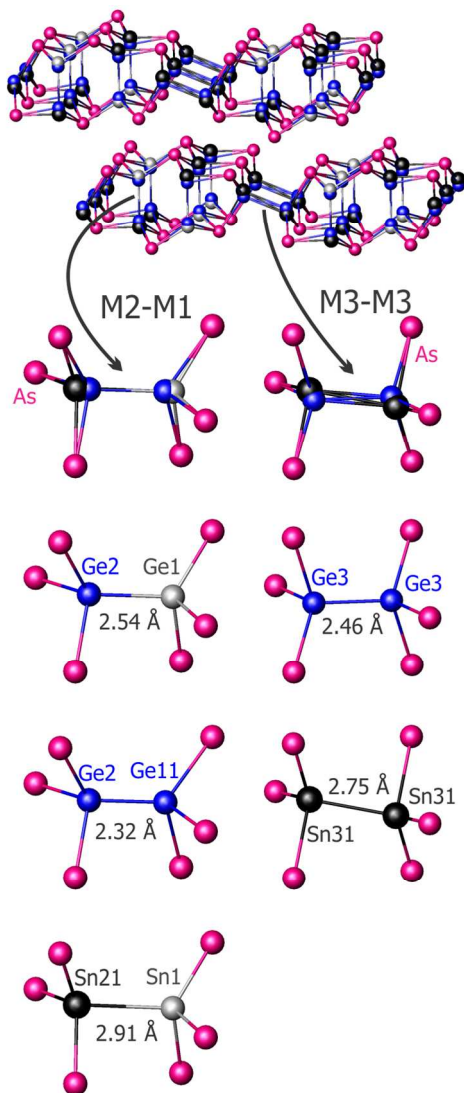


Figure 2. Top: Average model of the crystal structure of Sn-doped GeAs. Bottom: Enlarged local coordination of bimetallic dumbbells showing chemically reasonable possibilities together with interatomic distances. Sn: black, Ge: blue, mixed Ge/Sn: grey, As: pink.

It should be kept in mind that the reported model is an oversimplification of a complicated disordered structure. It is reliably determined that in the Ge positions there are Ge+Sn atoms, but the distribution of Sn might be not as simple as we refined it to be (Figure 2). In our model, long metal-metal distances, $>2.75 \text{ \AA}$, were assigned to Sn-Sn bonds rather than Sn-Ge or Ge-Ge bonds. To verify this assumption ^{119}Sn Mössbauer spectroscopy was applied, which is sensitive to the local tin coordination to further refine our model. Samples of Sn-doped GeAs grown from Sn flux were used to ensure the highest concentrations of Sn in the sample. The spectrum could be fitted with only one doublet with an isomer shift of $1.68 \text{ mm}\cdot\text{s}^{-1}$ and a small quadrupole splitting of $0.44 \text{ mm}\cdot\text{s}^{-1}$ (Figure 3, top). Despite a scattered spectrum due to the low Sn concentration and sample self-absorption, the extracted hyperfine parameters give valuable information about the electronic state of the Sn atoms and their environment. The isomer shift value is characteristic for Sn that is metallic in nature. The low value of the quadrupole splitting indicates a relatively high symmetry around the Sn atoms. The linewidth is relatively narrow, which is an indication that the Sn atoms have a very homogeneous surrounding. While the spectrum can be fitted with a singlet, this is not probable as a singlet generally arises from Sn atoms in a highly symmetric cubic local symmetry.

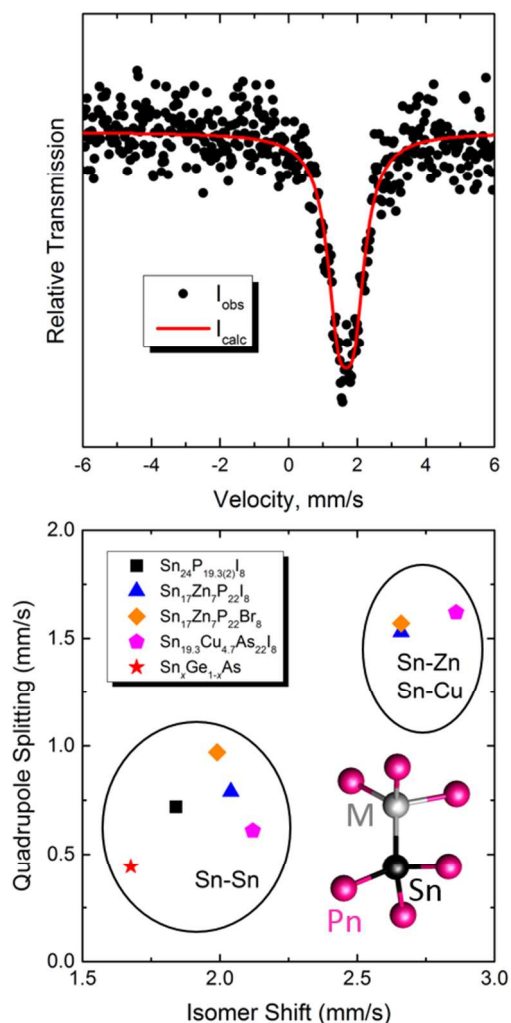


Figure 3. Top: ^{119}Sn Mössbauer spectrum of Sn-doped GeAs. Bottom: Comparison of quadrupole splittings and isomer shifts of Sn-metal bonds in Sn-M@ Pn_6 and Sn-Sn@ Pn_6 fragments. For the quaternary compounds, Mössbauer data were taken from the listed references: $\text{Sn}_{24}\text{P}_{19.3(2)}\text{I}_8$,⁴¹ $\text{Sn}_{17}\text{Zn}_7\text{P}_{22}\text{I}_8$,⁴² $\text{Sn}_{17}\text{Zn}_7\text{P}_{22}\text{Br}_8$,⁴² and $\text{Sn}_{19.3}\text{Cu}_{4.7}\text{As}_{22}\text{I}_8$.⁴³

A large set of clathrate compounds where similar fragments involving Sn atoms are present was characterized with ^{119}Sn Mössbauer spectroscopy.⁴¹⁻⁴³ In these clathrates, metal dumbbells, Sn-Sn or Sn-M (M = Zn, Cu), are situated inside distorted antiprisms of pnictogen atoms, P_6 or As_6 (Figure 3, bottom). Sn atoms bonded to Zn or Cu atoms showed larger isomer shifts and larger quadrupole splittings due to the asymmetry of the environment and strong electronic density redistribution. In turn, tin atoms from Sn_2 dumbbells displayed small isomer shifts and quadrupole splittings (Figure 3, bottom). Sn-doped GeAs possessed even smaller isomer shifts and quadrupole splittings, indicating that the Sn atoms are located in highly symmetric environments and present in the GeAs structure as Sn-Sn pairs.

This example shows the importance of the investigation of the local structure.^{44,45} While doping is often used in material science to modify materials' properties, the exact

positions, coordination, and chemical bonding of the dopants are scarcely studied, which hampers the establishment of proper structure-properties relationships.

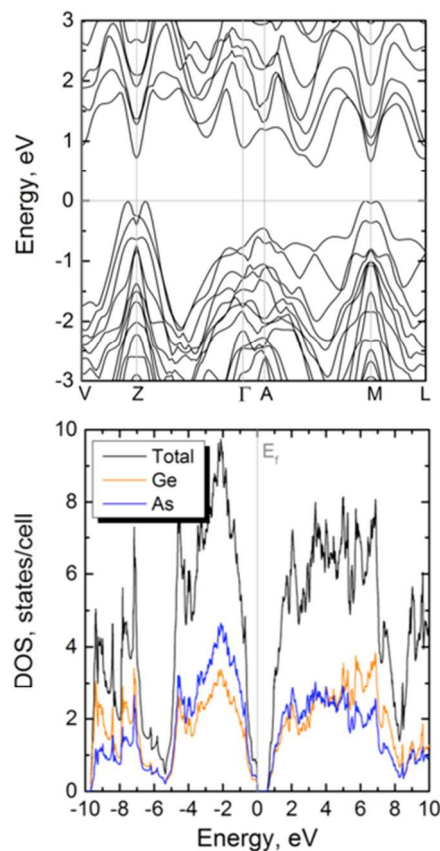


Figure 4. Band structure (top) and density of states (bottom) for GeAs.

ELECTRONIC STRUCTURE According to the band structure and density of states (DOS), GeAs is a narrow bandgap semiconductor with an indirect bandgap of 0.57 eV (Figure 4). The direct transition at the M point, 0.70 eV, is similar in energy to the indirect transitions in the vicinity of the Z point (Figure 4, top). The calculated bandgap is in good agreement with an optical bandgap measurement of 0.65 eV.⁴⁶ Both Ge and As contribute equally to the states in the conduction band with a slightly higher contribution of As orbitals to the states in the top of the valence band (Figure 4, bottom). A steep increase of the DOS near the Fermi level is calculated indicating the possibility for high thermopower. ELF analysis indicates strong covalent Ge-Ge and Ge-As bonding as well as the presence of electron lone pairs on all terminal As atoms, similar to GeP^{24} (Figure S4). No interlayer bonding was detected.

THERMOELECTRIC PROPERTIES The electrical resistivity, thermal conductivity, and Seebeck coefficients were measured for an oriented crystal and pellets at low temperature (LT) (2-400 K). The high temperature (HT) properties in the range of 300-723 K were measured on a Sn-doped sample with the nominal composition $\text{Sn}_{0.03}\text{Ge}_{0.97}\text{As}$. The Sn-doped sample had improved

mechanical properties such that large diameter pellets could be pressed with lower pressures than for pure GeAs. We were unable to press large diameter pellets of GeAs with high enough densities for properties measurements. Growth of large single crystals and investigation of alternative pressing methods to produce large crystals and pellets suitable for HT measurements are currently underway.

As expected from the crystal structure, GeAs exhibits anisotropic properties when measured along the layers and across the layers. The covalent bonding network within each of the layers is an effective conductor of charge carriers and heat-carrying phonons, while van der Waals gaps between the layers serve as effective scatterers of both carriers. The resistivity of GeAs along the layers (\parallel -GeAs) is over two orders of magnitude lower than the resistivity perpendicular to the layers (\perp -GeAs), 44.3 m Ω ·cm and 1520 m Ω ·cm, respectively at 300 K (Figure 5, top). The resistivity of GeAs measured along the crystallographic layers is within the previously reported range of 20-200 m Ω ·cm at 300 K.⁴⁶ The resistivity of the GeAs pellet substantially deviates from the statistical average of $2/3\rho_{\parallel} + 1/3\rho_{\perp}$, thus indicating the presence of texturing in the pellet. Because GeAs grows as plate-like crystals, the spark plasma sintering process does not ensure a completely random orientation of particles, and instead the plate-like crystallites may stack in a manner that is similar to the layered crystal structure.

The anisotropy in transport properties is also exhibited in the thermal conductivity. The thermal conductivity of GeAs in the parallel orientation is over an order of magnitude larger than the thermal conductivity of GeAs in the perpendicular orientation at room temperature, 12.6 and 0.4 W·m⁻¹·K⁻¹, respectively (Figure 5, bottom left). Using the Wiedemann-Franz law, the total thermal conductivity can be separated into electronic and lattice contributions. The lattice contribution to the total thermal conductivity dominates with minor contribution from the charge carriers (Figure S5). The thermal conductivity of \perp -GeAs at 300 K is comparable to the thermal conductivities of state-of-the-art thermoelectric materials and materials with ultralow thermal conductivities, such as Yb₁₄MnSb₁₁ (0.7 W·m⁻¹·K⁻¹),⁴⁷ Bi_{0.5}Sb_{1.5}Te₃ (0.7 W·m⁻¹·K⁻¹),⁴⁸ Ba₈Au₁₆P₃₀ (0.6 W·m⁻¹·K⁻¹),⁴⁹ and SnSe (0.46 W·m⁻¹·K⁻¹ for the [100] direction).¹³

Unlike the thermal conductivity and electrical resistivity, the Seebeck coefficients were more isotropic in both directions, 194 μ V·K⁻¹ and 150 μ V·K⁻¹ at 300 K for \parallel -GeAs and \perp -GeAs, respectively (Figure 5, top right). The pellet exhibited slightly higher thermopower than either direction, 231 μ V·K⁻¹ at 300 K. The positive values of the thermopower indicate that holes are the main charge carriers. The overall figure of merit increases by over an order of magnitude at room temperature from \perp -GeAs to

\parallel -GeAs (Figure 5, bottom right). While the GeAs pellet is more resistive than the GeAs crystal oriented in the parallel direction and has a similar Seebeck coefficient as the crystal oriented in either direction, the main gain to the figure of merit stems from the low thermal conductivity. The thermal conductivity of the pellet, while greater than the thermal conductivity of \perp -GeAs, is over an order of magnitude smaller than the GeAs crystal oriented in the parallel direction, giving an overall figure of merit of 0.01 at 300K. This is a two orders of magnitude increase from the figure of merit of the GeAs crystal oriented in the perpendicular direction. The GeAs example illustrates the necessity of characterization of the anisotropic properties of layered thermoelectric materials to achieve a complete understanding of thermoelectric properties.

The thermoelectric properties of compounds with anisotropic crystal structures have been previously reported. Theory suggests extreme anisotropy for single layer materials such as graphene, phosphorene, and arsenene.¹² Bulk thermoelectric materials, Sb₂Te₃,⁵⁰ PbSb₂Te₄,⁵¹ PbBi₄Te₇,⁵¹ and SnSe,¹³ all show anisotropic properties in the thermopower, resistivity, and thermal conductivity. Table 2 summarizes the thermal and electronic transport properties of these compounds in comparison with GeAs. Like GeAs, Sb₂Te₃ has similar values for the Seebeck coefficient in both crystallographic directions and anisotropic resistivity and thermal conductivity values. PbSb₂Te₄, PbBi₄Te₇, and SnSe exhibit higher anisotropy than Sb₂Te₃ in the electrical resistivity and thermal conductivity, with an order of magnitude difference in the figure of merit at room temperature. GeAs has the largest anisotropy in the thermal conductivity compared to the listed materials, with the exception of graphite. Like graphite, which shows 2-3 orders of magnitude difference in electrical conductivity along the layers versus perpendicular to the layers, GeAs also shows high anisotropy in conductivity. The high electrical conductivity coupled with high thermal conductivity for \parallel -GeAs resulted in a figure of merit similar to \perp -GeAs with the low electrical conductivity and low thermal conductivity.

Sn doping improves the overall figure of merit for GeAs. The resistivity of Sn-doped GeAs pellet was slightly lower than the pure GeAs pellet resistivity reaching a value of 67 m Ω ·cm at 300 K (Figure 6, top left). The thermal conductivity of the Sn_xGe_{1-x}As pellet was slightly higher than thermal conductivity of pure GeAs (Figure 6, bottom left). At 300 K, the Seebeck coefficient for the Sn_xGe_{1-x}As pellet is similar to the thermopower of pure GeAs. The overall figure of merit for the Sn_xGe_{1-x}As pellet at 300 K is 0.02, a factor of two increase compared to the pure GeAs pellet.

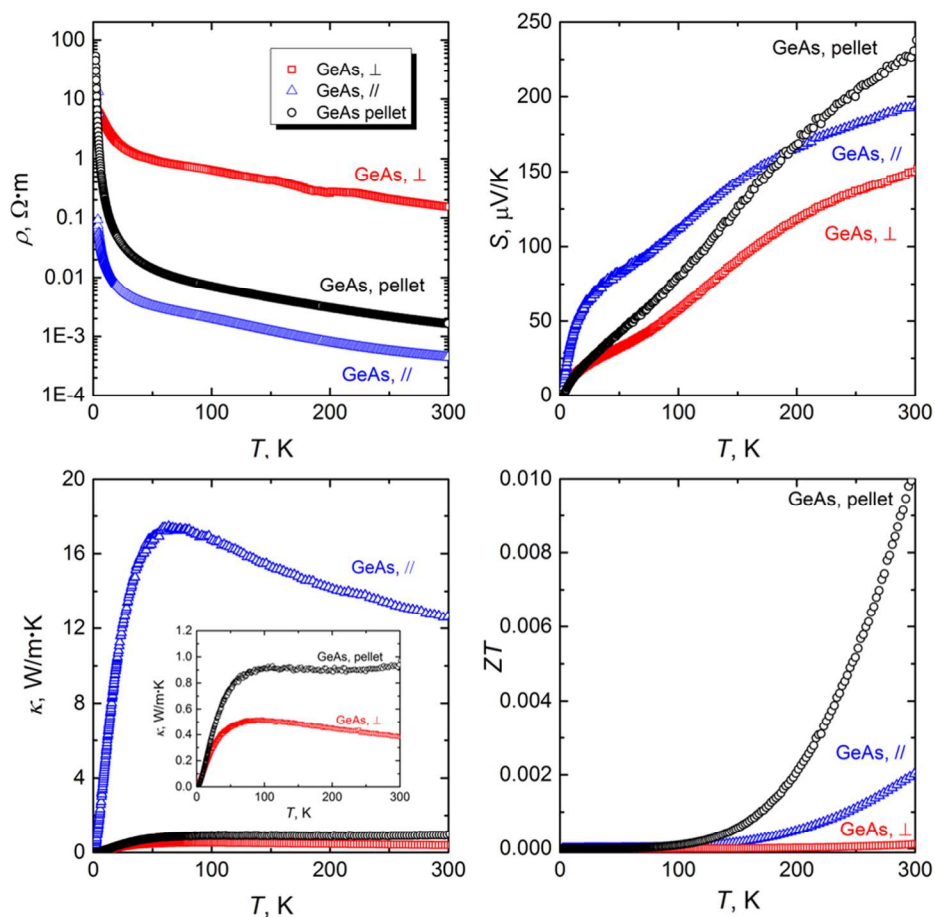


Figure 5. Top left: resistivity; top right: Seebeck coefficient; bottom left: thermal conductivity; and bottom right: figure of merit plots for the GeAs pellet and the GeAs crystal measured parallel and perpendicular to the GeAs layers.

Table 2. Anisotropic thermoelectric properties at 300 K for selected layered compounds.

Compound, direction	S ($\mu\text{V}\cdot\text{K}^{-1}$)	σ ($\text{S}\cdot\text{cm}^{-1}$)	$\sigma_{\parallel}/\sigma_{\perp}$	κ ($\text{W}\cdot\text{m}^{-1}\cdot\text{K}^{-1}$)	$\kappa_{\parallel}/\kappa_{\perp}$	ZT
$^{50}\text{Sb}_2\text{Te}_3$, parallel	73	4150	1.8	4600	1.8	1.4×10^{-4}
$^{50}\text{Sb}_2\text{Te}_3$, perpendicular	90	2340		2620		2.2×10^{-4}
$^{51}\text{PbSb}_2\text{Te}_4$ (SbI_3 doped), parallel	26	2354	10.1	2910	4.5	1.6×10^{-5}
$^{51}\text{PbSb}_2\text{Te}_4$ (SbI_3 doped), perpendicular	107	232		650		1.2×10^{-4}
$^{51}\text{PbBi}_4\text{Te}_7$, parallel	-18	3358	4.3	4150	3.8	7.9×10^{-6}
$^{51}\text{PbBi}_4\text{Te}_7$, perpendicular	-40	784		1090		3.5×10^{-5}
$^{13}\text{SnSe}$, parallel	510	10	5	0.7	1.5	0.2
$^{13}\text{SnSe}$, perpendicular	540	2		0.46		0.03
$^{52,53}\text{Graphite}$, parallel	--	2000-4000	606-1212	140-500	47-50	--
$^{52,53}\text{Graphite}$, perpendicular	--	3:3		3-10		--
$^a\text{GeAs}$, parallel	194	22.6	342:3	12.6	33.2	0.002
$^a\text{GeAs}$, perpendicular	159	0.066		0.38		0.001

^a This work.

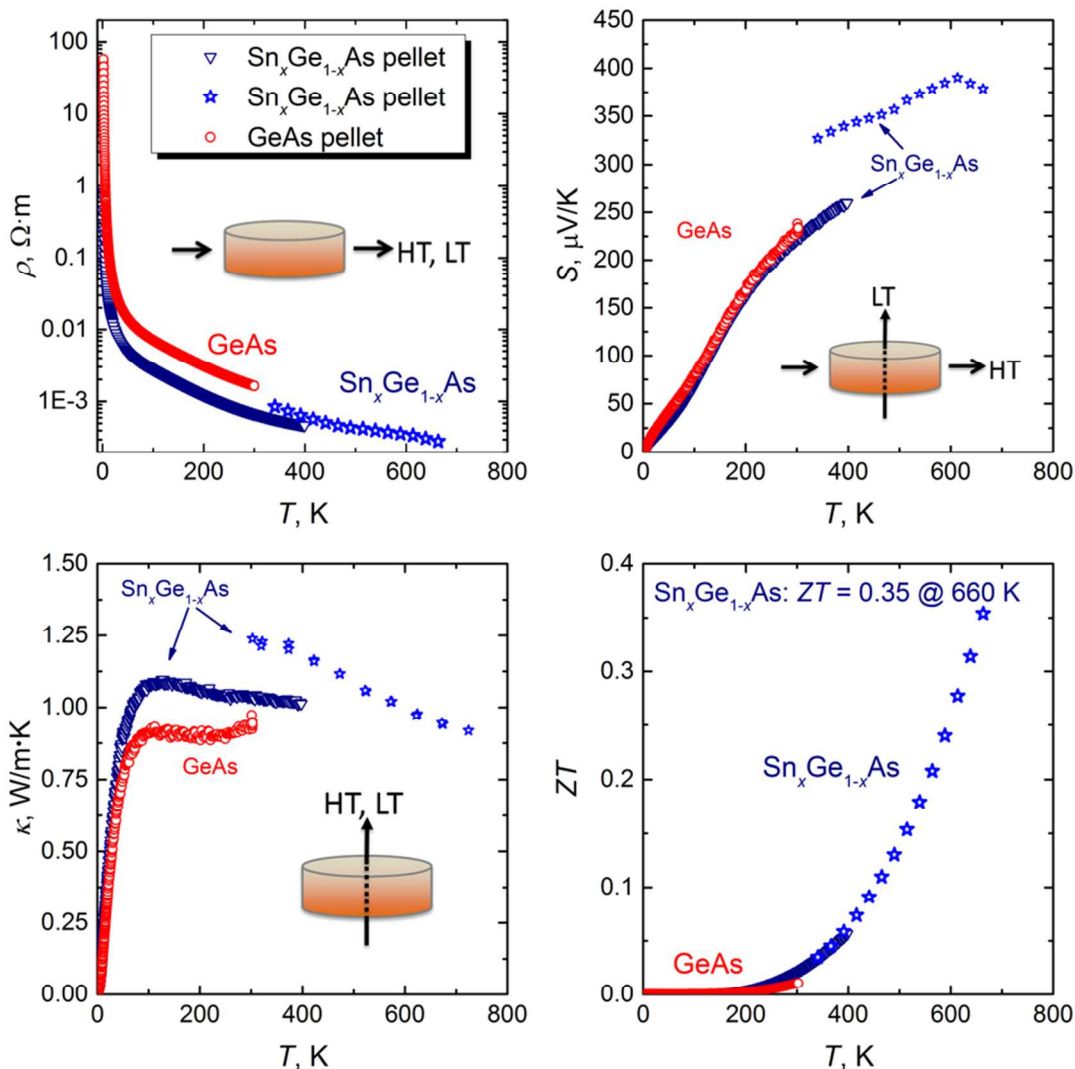


Figure 6. Top left: resistivity; top right: Seebeck coefficient; bottom left: thermal conductivity; and bottom right: figure of merit plots for GeAs and Sn_xGe_{1-x}As pellets. LT data are shown as circles and triangles and high temperature data are shown as blue stars.

At high temperatures the thermal conductivity of the Sn_xGe_{1-x}As pellet continues to decrease reaching a value of $0.92 \text{ W}\cdot\text{m}^{-1}\cdot\text{K}^{-1}$ at 777 K (Figure 6, bottom left). The small discrepancies of the resistivity and thermal conductivity values may be due to the fact that the LT and HT measurements were performed on different instruments. Moreover, each measurement was performed on the pellet that was oriented in different directions, which may result in alteration of properties assuming preferred orientation of the Sn_xGe_{1-x}As crystallites within the pellet (insets in Figure 6). The HT and LT thermal conductivity measurements were performed perpendicular to the pellet (parallel to the pressing direction), while the HT and LT resistivity measurements were performed across the pellet (perpendicular to the pressing direction). The Seebeck coefficients were similar at low temperatures and were measured perpendicular to the pellet for both GeAs and Sn_xGe_{1-x}As pellets. However, the HT measurements were performed across the pellet, which may explain the discrepancy in Seebeck coefficient values. The Seebeck coefficient for Sn_xGe_{1-x}As reaches a maximum value of 390

$\mu\text{V}\cdot\text{K}^{-1}$ at 605 K, indicating a bipolar state with two different types of charge carriers (Figure 6, top right). A Goldsmid-Sharp bandgap estimation⁵⁴ as $E_g = 2e|S_{\text{max}}|T_{\text{max}} = 0.47 \text{ eV}$ is slightly smaller than the values for undoped GeAs predicted by quantum chemical calculations, 0.57 eV, and the measured optical bandgap of 0.65 eV.⁴⁶

Due to the high Seebeck thermopower and low thermal conductivity, the Sn_xGe_{1-x}As pellet exhibits a peak ZT value of 0.35 at 660 K. This shows the general promise of layered van der Waals compounds, which are small bandgap semiconductors, for high temperature thermoelectric applications.

CONCLUSION GeAs and Sn-doped GeAs were synthesized and the crystal structures, electronic structure, as well as the transport properties were investigated. The anisotropy in the crystal structure is reflected in the transport properties with orders of magnitude difference in the resistivity of GeAs along the layers as opposed to perpendicular to the layers. The anisotropy is also reflected in the thermal conductivity as

the van der Waals gaps effectively inhibit phonon propagation. For the single crystal, the improved charge carrier transport causes the ZT along the layers to be an order of magnitude larger than the ZT across the layers. Investigation of the compacted polycrystalline pellets indicates that below room temperature, Sn-doped GeAs exhibits similar transport properties as the pristine GeAs. At high temperatures Sn-doped GeAs reaches a peak ZT of 0.35 at 660 K. Studies of other tetrel-pnictides as well as growth of large single crystals to characterize anisotropic transport properties are currently underway.

ASSOCIATED CONTENT

Supporting Information

Supporting Information includes tables containing selected bond distances and atomic coordinates, powder XRD patterns, DSC pots, EDX spectra, ELF isosurface and slice, lattice and electronic contributions to the thermal conductivity.

The Supporting Information is available free of charge on the ACS Publications website.

AUTHOR INFORMATION

Corresponding Author

*Kirill Kovnir. Tel.: +1 530 752 5563; fax: +1 530 752 8995;
Email address: kkovnir@ucdavis.edu

Notes

The authors declare no competing financial interest.

ACKNOWLEDGMENT

We thank Prof. S. M. Kauzlarich for access to the DSC, Linseis, LFA, and SPS. We thank Katherine Woo for assistance with X-ray powder diffraction measurements, Yufei Hu for assistance with high temperature TE measurements, and Joya Cooley for helpful discussions regarding the SPS. KL acknowledges the GAANN and ARCS fellowships. This research is supported by the U.S. Department of Energy, Office of Basic Energy Sciences, Division of Materials Sciences and Engineering under Award DE-SC0008931.

REFERENCES

- (1) Slack, G. A. *CRC Handbook of Thermoelectrics*; Rowe, M., Ed. CRC Press: Boca Raton, FL, 1995, pp 407-440.
- (2) Dolyniuk, J.-A.; Wang, J.; Lee, K.; Kovnir, K. Twisted Kelvin Cells and Truncated Octahedral Cages in the Crystal Structures of Unconventional Clathrates, AM_2P_4 (A = Sr, Ba; M = Cu, Ni) *Chem. Mater.* **2015**, *27*, 4476-4484.
- (3) *The Physics and Chemistry of Inorganic Clathrates*; Nolas, G., Ed. Springer: Dordrecht, Netherlands, 2014.
- (4) A.V. Shevelkov; Kovnir K. Zintl Clathrates. In *Principles and Recent Developments in the field of Zintl Ions and Zintl Phases Structure & Bonding*, Fassler, T. F., Ed., Springer **2011**, *139*, 97-142.
- (5) Snyder, G. J.; Christensen, M.; Nishibori, E.; Caillat, T.; Iversen, B. B. Disordered Zinc in Zn_4Sb_3 with Phonon-Glass and

Electron-Crystal Thermoelectric Properties *Nature Mater.* **2004**, *3*, 458-463.

(6) Wang, J.; Kovnir, K. Elusive β - Zn_8Sb_7 : A New Zinc Antimonide Thermoelectric *J. Am. Chem. Soc.* **2015**, *137*, 12474-12477.

(7) Zhang, C.; Peng, Z.; Li, Z.; Yu, L.; Khor, K. A.; Xiong, Q. Controlled Growth of Bismuth Antimony Telluride $Bi_xSb_{2-x}Te_3$ Nanoplatelets and Their Bulk Thermoelectric Nanocomposites *Nano Energy* **2015**, *15*, 688-696.

(8) Kazem, N.; Zaikina, J. V.; Ohno, S.; Snyder, G. J.; Kauzlarich, S. M. Coinage-Metal-Stuffed $Eu_9Cd_4Sb_6$: Metallic Compounds with Anomalous Low Thermal Conductivities *Chem. Mater.* **2015**, *27*, 7508-7519.

(9) Skoug, E. J.; Morelli, D. T. Role of Lone-Pair Electrons in Producing Minimum Thermal Conductivity in Nitrogen-Group Chalcogenide Compounds *Phys. Rev. Lett.* **2011**, *107*, 235901.

(10) Wang, S.; Yang, J.; Wu, L.; Wei, P.; Yang, J.; Zhang, W.; Grin, Y. Anisotropic Multicenter Bonding and High Thermoelectric Performance in Electron-Poor CdSb *Chem. Mater.* **2015**, *27*, 1071-1081.

(11) Nielsen, M. D.; Ozolins, V.; Heremans, J. P. Lone Pair Electrons Minimize Lattice Thermal Conductivity *Energy Environ. Sci.* **2013**, *6*, 570-578.

(12) Liu, T.-H.; Chang, C.-C. Anisotropic Thermal Transport in Phosphorene: Effects of Crystal Orientation *Nanoscale* **2015**, *7*, 10648-10654.

(13) Zhao, L.-D.; Lo, S.-H.; Zhang, Y.; Sun, H.; Tan, G.; Uher, C.; Wolverton, C.; Dravid, V. P.; Kanatzidis, M. G. Ultralow Thermal Conductivity and High Thermoelectric Figure of Merit in SnSe Crystals *Nature* **2014**, *508*, 373-377.

(14) Sheldrick, G. A Short History of SHELX *Acta Cryst. A.* **2008**, *64*, 112-122.

(15) Jepsen, O.; Burkhardt, A.; Andersen, O. K. The Program TB-LMTO-ASA **1999**, Version 4.7; Max-Planck-Institut für Festkörperforschung: Stuttgart, Germany.

(16) Barth, U. v.; Hedin, L. A local exchange-correlation potential for the spin polarized case. i *Journal of Physics C: Solid State Physics* **1972**, *5*, 1629.

(17) Becke, A. D.; Edgecombe, K. E. A Simple Measure of Electron Localization in Atomic and Molecular Systems *J. Chem. Phys.* **1990**, *92*, 5397.

(18) Savin, A.; Jepsen, O.; Flad, J.; Andersen, O. K.; Preuss, H.; von Schnering, H. G. Electron Localization in Solid-State Structures of the Elements: the Diamond Structure *Angew. Chem. Int. Ed.* **1992**, *31*, 187-188.

(19) Savin, A.; Nesper, R.; Wengert, S.; Fässler, T. F. ELF: The Electron Localization Function *Angew. Chem. Int. Ed.* **1997**, *36*, 1808-1832.

(20) Lagarec, K.; Rancourt, D. C. Recoil, Mössbauer Spectral Analysis Software for Windows, 1.0; Department of Physics, University of Ottawa, Canada, 1998.

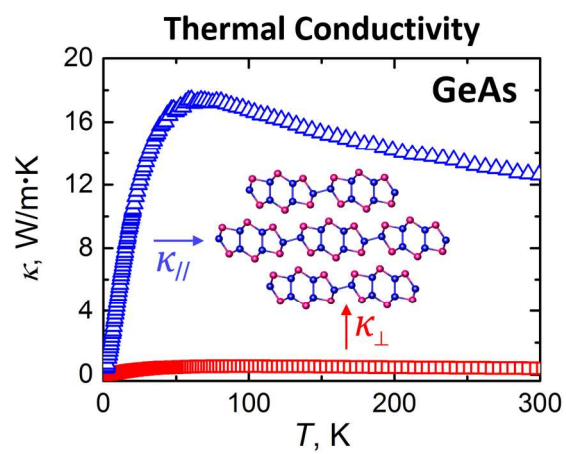
(21) Stöhr, H.; Klemm, W. Über Zweistoffsysteme mit Germanium. II. Germanium/Arsen, Germanium/Antimon, Germanium/Wismut *Z. Anorg. Allg. Chem.* **1940**, *244*, 205-223.

(22) Wadsten, T. Studies on the Thermal Decomposition of Phosphides and Arsenides of Silicon and of Germanium *Thermochim. Acta* **1977**, *21*, 285-290.

(23) Mentzen, B. F.; Hillel, R.; Michaelides, A.; Tranquard, A.; Bouix, J. Étude structurale du monoarséniure de germanium. *C. R. Acad. Sci. Paris* **1981**, *293*, 965-967.

(24) Lee, K.; Synnestvedt, S.; Bellard, M.; Kovnir, K. GeP and $(Ge_{1-x}Sn_x)(P_{1-y}Ge_y)$ ($x \approx 0.12$, $y \approx 0.05$): Synthesis, Structure, and

- Properties of Two-Dimensional Layered Tetrel Phosphides *J. Solid State Chem.* **2015**, *224*, 62-70.
- (25) Olesinski, R. W.; Abbaschian, G. J. The As-Ge (Arsenic-Germanium) System *Bull. Alloy Phase Diagr.* **1985**, *6*, 250-254.
- (26) Goncharov, E.G.; Gladyshev, N.F.; Ugai, Ya.A. Physicochemical Nature of Intermediate Phases in the Germanium-Arsenic System. *Russ. J. Inorg. Chem.* **1977**, *22*, 1059-1061.
- (27) Ugai, Ya. A.; Gladyshev, N.F.; Goncharov, E.G. Tensimetric Investigation of the As-Ge System. *Russ. J. Inorg. Chem.* **1978**, *23*, 589-591.
- (28) Blachnik, R.; Irle, E. Das System Gallium-Tellur *J. Less-Common Met.* **1985**, *113*, L1-L3.
- (29) Pfister, H. Kristallstruktur von Ternären Verbindungen der Art $A^{II}B^{IV}C^V$ *Acta Cryst.* **1958**, *11*, 221-224.
- (30) Eisenmann, B.; Schäfer, H. Zintl Phases with Binary Anions: $BaGe_2P_2$ and $BaGe_2As_2$. *Z. Naturforsch.* **1981**, *36b*, 415-419.
- (31) Eisenmann, B.; Schäfer, H. Neuartige Polyanionen in Zintlphasen. Zur Kenntnis von $Ca_3Si_2As_4$, $Ca_3Ge_2As_4$, $Sr_3Si_2As_4$ und $Sr_3Ge_2As_4$. *Z. Anorg. Allg. Chem.* **1982**, *484*, 142-152.
- (32) Eisenmann, B.; Schäfer, H. Zintl-Phasen mit Komplexen Anionen: $Sr_3Si_2As_4$ und $Sr_3Ge_2As_4$. *Angew. Chem.* **1980**, *92*, 480-481.
- (33) Menke, H.; von Schnering, H. G. Die Käfigverbindungen $Ge_{38}Ax_8$ mit $A = P, As, Sb$ und $X = Cl, Br, I$. *Z. Anorg. Allg. Chem.* **1973**, *395*, 223-238.
- (34) Kovnir, K.A.; Abramchuk, N.S.; Zaikina, J.V.; Baitinger, M.; Burkhardt, U.; Schnelle, W.; Olenev, A.V.; Lebedev, O.I.; Van Tendeloo, G.; Dikarev, E.V.; Shevelkov, A.V. $Ge_{40.0}Te_{5.3}I_8$: Synthesis, Crystal Structure, and Properties of a New Clathrate-I Compound. *Z. Kristallogr.* **2006**, *221*, 527-532.
- (35) Schnering, H. G. v.; Kröner, R.; Carrillo-Cabrera, W.; Peters, K.; Nesper, R. Crystal structure of the novel chiral clathrate, $Ba_6In_4Ge_{21}$. *Z. Kristallogr. -New Cryst. Struct.* **1998**, *213*, 665-666.
- (36) Zhang, H.; Borrmann, H.; Oeschler, N.; Candolfi, C.; Schnelle, W.; Schmidt, M.; Burkhardt, U.; Baitinger, M.; Zhao, J.-T.; Grin, Y. Atomic Interactions in the p-Type Clathrate I $Ba_8Au_{5.3}Ge_{40.7}$. *Inorg. Chem.* **2011**, *50*, 1250-1257.
- (37) Zhang, J.; Tobash, P. H.; Pryz, W. D.; Buttey, D. J.; Hur, N.; Thompson, J. D.; Sarrao, J. L.; Bobev, S. Synthesis, Structural Characterization, and Physical Properties of the Early Rare-Earth Metal Digermanides $REGe_{2-x}$ ($x \approx 1/4$) [RE = La-Nd, Sm]. A Case Study of Commensurately and Incommensurately Modulated Structures *Inorg. Chem.* **2013**, *52*, 953-964.
- (38) Schlüter, M.; Häussermann, U.; Heying, B.; Pöttgen, R. Tin-Magnesium Substitution in Ir_3Sn_7 —Structure and Chemical Bonding in $Mg_xIr_3Sn_{7-x}$ ($x=0-1.67$) *J. Solid State Chem.* **2003**, *173*, 418-424.
- (39) Stefanoski, S.; Dong, Y.; Nolas, G. S. Structural Characterization and Low-Temperature Physical Properties of p-Type Single-Crystal $K_8Ga_{8.5}Sn_{37.5}$ Grown by Self-Flux Method *J. Solid State Chem.* **2013**, *204*, 166-169.
- (40) Zaikina, J. V.; Kovnir, K. A.; Sobolev, A. V.; Presniakov, I. A.; Prots, Y.; Baitinger, M.; Schnelle, W.; Olenev, A. V.; Lebedev, O. I.; Van Tendeloo, G.; Grin, Y.; Shevelkov, A. V. $Sn_{20.5}□_{3.5}As_{22}I_8$: A Largely Disordered Cationic Clathrate with a New Type of Superstructure and Abnormally Low Thermal Conductivity *Chem. Eur. J.* **2007**, *13*, 5090-5099.
- (41) Shatruk, M. M.; Kovnir, K. A.; Shevelkov, A. V.; Presniakov, I. A.; Popovkin, B. A. First Tin Pnictide Halides $Sn_{24}P_{19-3}I_8$ and $Sn_{24}As_{19-3}I_8$: Synthesis and the Clathrate-I Type of the Crystal Structure *Inorg. Chem.* **1999**, *38*, 3455-3457.
- (42) Kovnir, K. A.; Shatruk, M. M.; Reshetova, L. N.; Presniakov, I. A.; Dikarev, E. V.; Baitinger, M.; Haarmann, F.; Schnelle, W.; Baenitz, M.; Grin, Y.; Shevelkov, A. V. Novel Compounds $Sn_{20}Zn_4P_{22-v}I_8$ ($v=1,2$), $Sn_{17}Zn_7P_{22}I_8$, and $Sn_{17}Zn_7P_{22}Br_8$: Synthesis, Properties, and Special Features of Their Clathrate-Like Crystal Structures *Solid State Sci.* **2005**, *7*, 957-968.
- (43) Kovnir, K. A.; Sobolev, A. V.; Presniakov, I. A.; Lebedev, O. I.; Van Tendeloo, G.; Schnelle, W.; Grin, Y.; Shevelkov, A. V. $Sn_{19.3}Cu_{4.7}As_{22}I_8$: A New Clathrate-I Compound with Transition-Metal Atoms in the Cationic Framework *Inorg. Chem.* **2005**, *44*, 8786-8793.
- (44) Lee, K.; Kaseman, D.; Sen, S.; Hung, I.; Gan, Z.; Gerke, B.; Pöttgen, R.; Feygenson, M.; Neufelnd, J.; Lebedev, O. I.; Kovnir, K. Intricate Short-Range Ordering and Strongly Anisotropic Transport Properties of $Li_{1-x}Sn_{2+x}As_2$. *J. Am. Chem. Soc.* **2015**, *137*, 3622-3630.
- (45) Greenfield, J. T.; Kamali, S.; Lee, K.; Kovnir, K. A. Solution for Solution-Produced β -FeSe: Elucidating and Overcoming Factors that Prevent Superconductivity *Chem. Mater.* **2015**, *27*, 588-596.
- (46) Rau, J. W.; Kannewurf, C. R. Optical Absorption, Reflectivity, and Electrical Conductivity in GeAs and GeAs₂. *Phys. Rev. B* **1971**, *3*, 2581-2587.
- (47) Brown, S. R.; Kauzlarich, S. M.; Gascoin, F.; Snyder, G. J. $Yb_{14}MnSb_{11}$: New High Efficiency Thermoelectric Material for Power Generation *Chem. Mater.* **2006**, *18*, 1873-1877.
- (48) Poudel, B.; Hao, Q.; Ma, Y.; Lan, Y.; Minnich, A.; Yu, B.; Yan, X.; Wang, D.; Muto, A.; Vashaee, D.; Chen, X.; Liu, J.; Dresselhaus, M. S.; Chen, G.; Ren, Z. High-Thermoelectric Performance of Nanostructured Bismuth Antimony Telluride Bulk Alloys *Science* **2008**, *320*, 634-638.
- (49) Fulmer, J.; Lebedev, O. I.; Roddatis, V. V.; Kaseman, D. C.; Sen, S.; Dolyniuk, J.-A.; Lee, K.; Olenev, A. V.; Kovnir, K. Clathrate $Ba_8Au_{16}P_{30}$: The "Gold Standard" for Lattice Thermal Conductivity *J. Am. Chem. Soc.* **2013**, *135*, 12313-12323.
- (50) Ivanova, L. D., Granatkina, Yu.V., and Sidorov, Yu.A. Electrical Properties of Antimony Telluride Crystals Doped with Selenium and Bismuth *Neorg. Mater.* **1999**, *35*, 44-52.
- (51) Shelimova, L. E.; Svechnikova, T. E.; Konstantinov, P. P.; Karpinskii, O. G.; Avilov, E. S.; Kretova, M. A.; Zemskov, V. S. Anisotropic Thermoelectric Properties of the Layered Compounds $PbSb_2Te_4$ and $PbBi_4Te_7$. *Inorg. Mater.* **2007**, *43*, 125-131.
- (52) Pierson, H. O. *Handbook of Carbon, Graphite, Diamond, and Fullerenes: Properties, Processing, and Applications* Noyes Publications: Park Ridge, NJ, 1993, pp 61.
- (53) Smalc, M.; Shives, G.; Chen, G.; Guggari, S.; Norley, J.; Reynolds III, R. A. Paper presented at ASME 2005 Pacific Rim Technical Conference and Exhibition on Integration and Packaging of MEMS, NEMS, and Electronic Systems colocated with the ASME 2005 Heat Transfer Summer Conference. Thermal Performance of Natural Graphite Heat Spreaders. **2005**, San Francisco, CA, 17-22 July (pp. 79-89) ASME Proceedings.
- (54) Goldsmid, H. J.; Sharp, J. W. Estimation of the Thermal Band Gap of a Semiconductor from Seebeck Measurements *J. Electron. Mater.* **1999**, *28*, 869-872



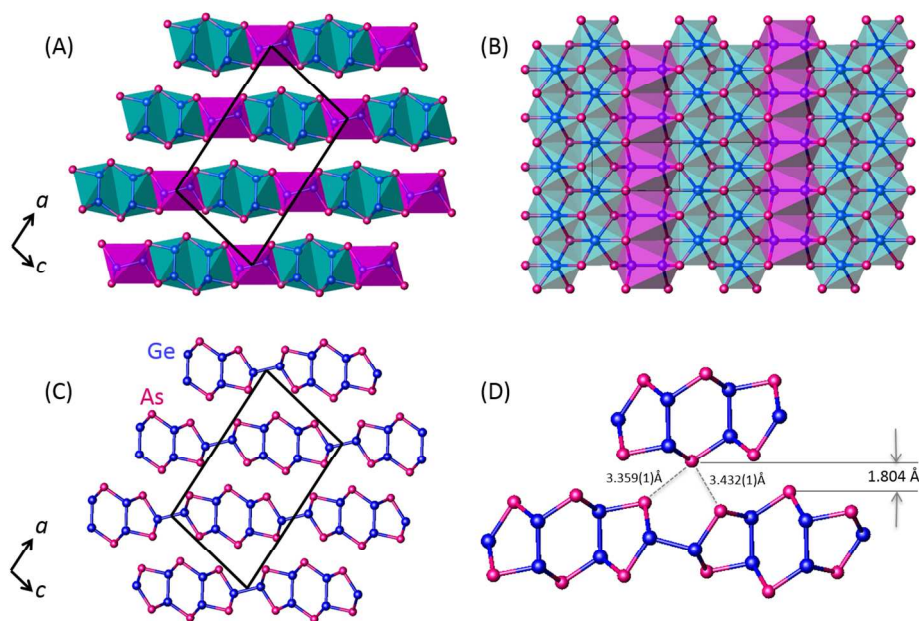


Figure 1. Crystal structure of GeAs. A. Polyhedral view; B. top view of a single layer; C. ball-and stick model; (D) fragment of GeAs showing shortest As-As distances and interlayer spacing. Ge: blue; As: red; Ge₂@As₆ polyhedra: green and pink.
251x163mm (150 x 150 DPI)

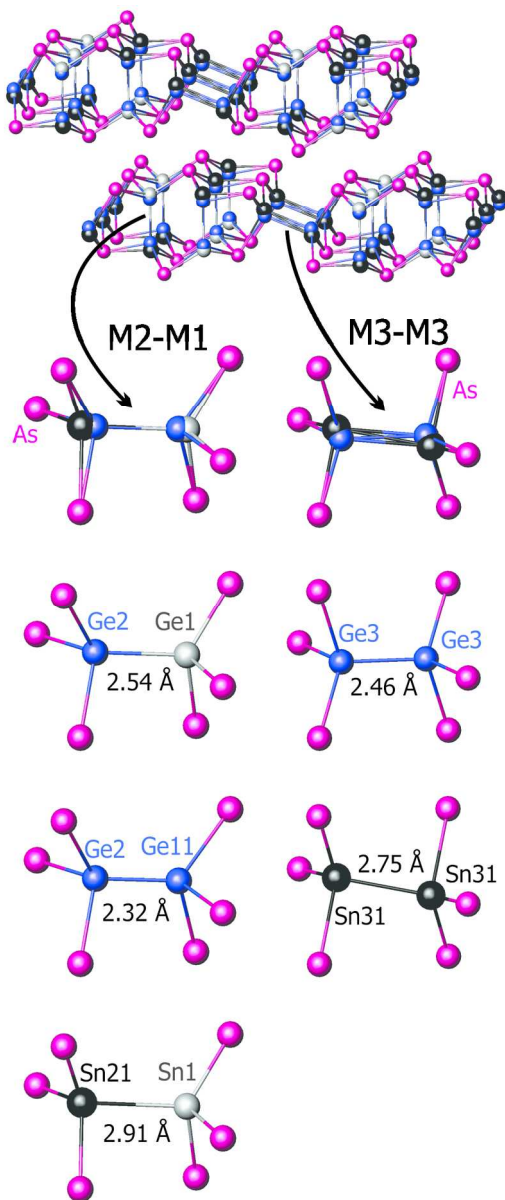


Figure 2. Top: Average model of the crystal structure of Sn-doped GeAs. Bottom: Enlarged local coordination of bimetallic dumbbells showing chemically reasonable possibilities together with interatomic distances. Sn: black, Ge: blue, mixed Ge/Sn: grey, As: pink.
89x203mm (299 x 299 DPI)

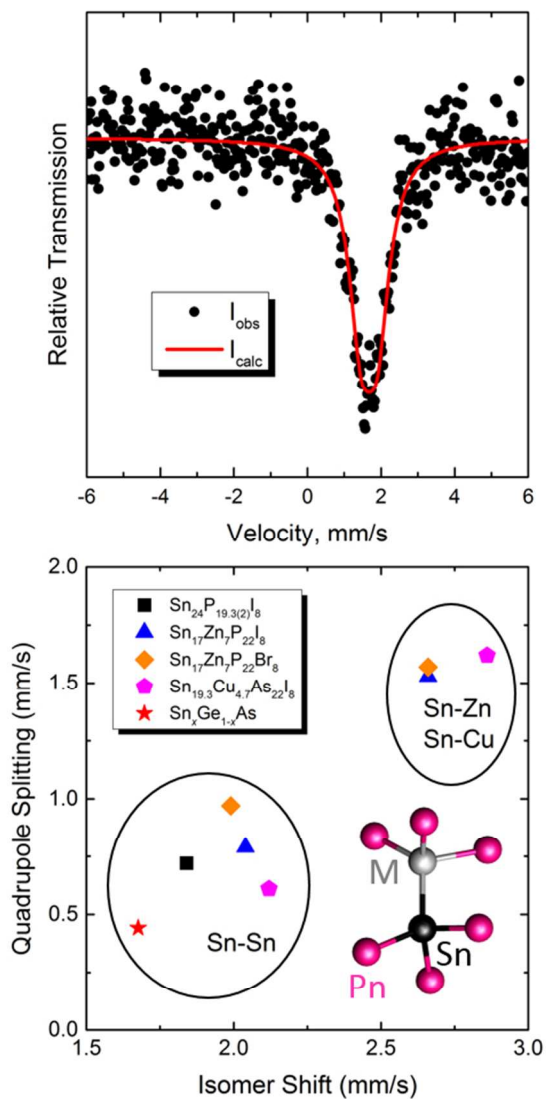


Figure 3. Top: ^{119}Sn Mössbauer spectrum of Sn-doped GeAs. Bottom: Comparison of quadrupole splittings and isomer shifts of Sn-metal bonds in Sn-M@Pn6 and Sn-Sn@Pn6 fragments. For the quaternary compounds, Mössbauer data were taken from the listed references: Sn24P19.3(2)I8 [29], Sn17Zn7P22I8 [30], Sn17Sn7P22Br8 [30], Sn19.3Cu4.7As22I8 [31].

95x177mm (150 x 150 DPI)

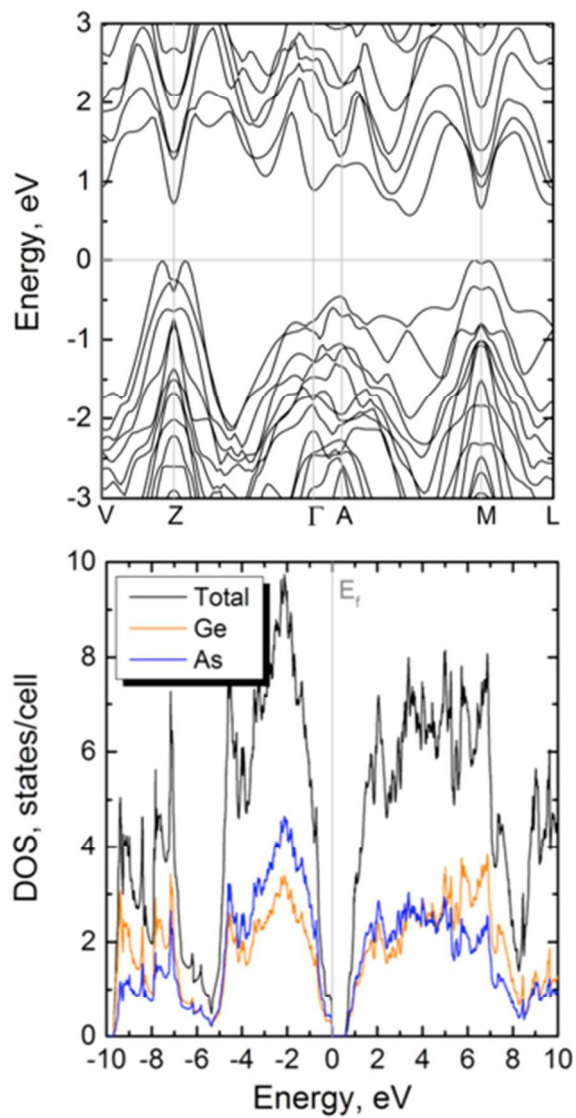


Figure 4. Band structure (top) and density of states (bottom) for GeAs.
68x123mm (150 x 150 DPI)

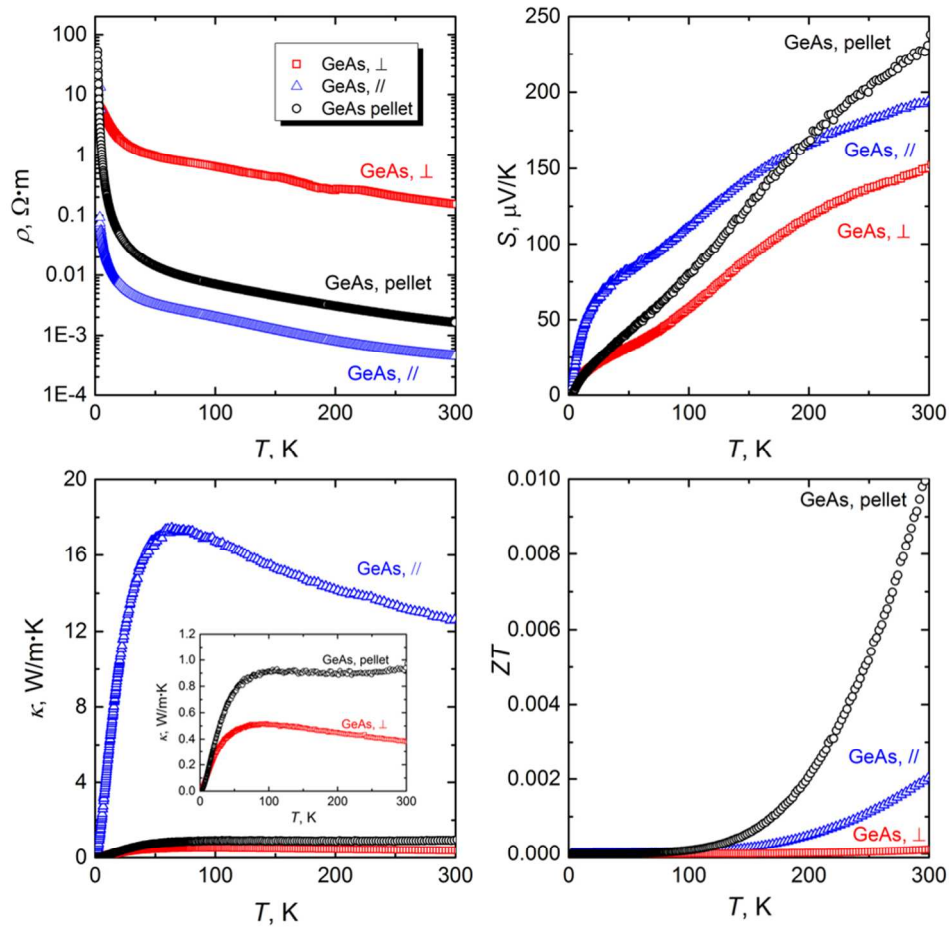


Figure 5. Top left: resistivity; Top right: Seebeck coefficient; Bottom left: thermal conductivity; and Bottom right: figure-of-merit plots for the GeAs pellet and the GeAs crystal measured parallel and perpendicular to the GeAs layers.
192x190mm (150 x 150 DPI)

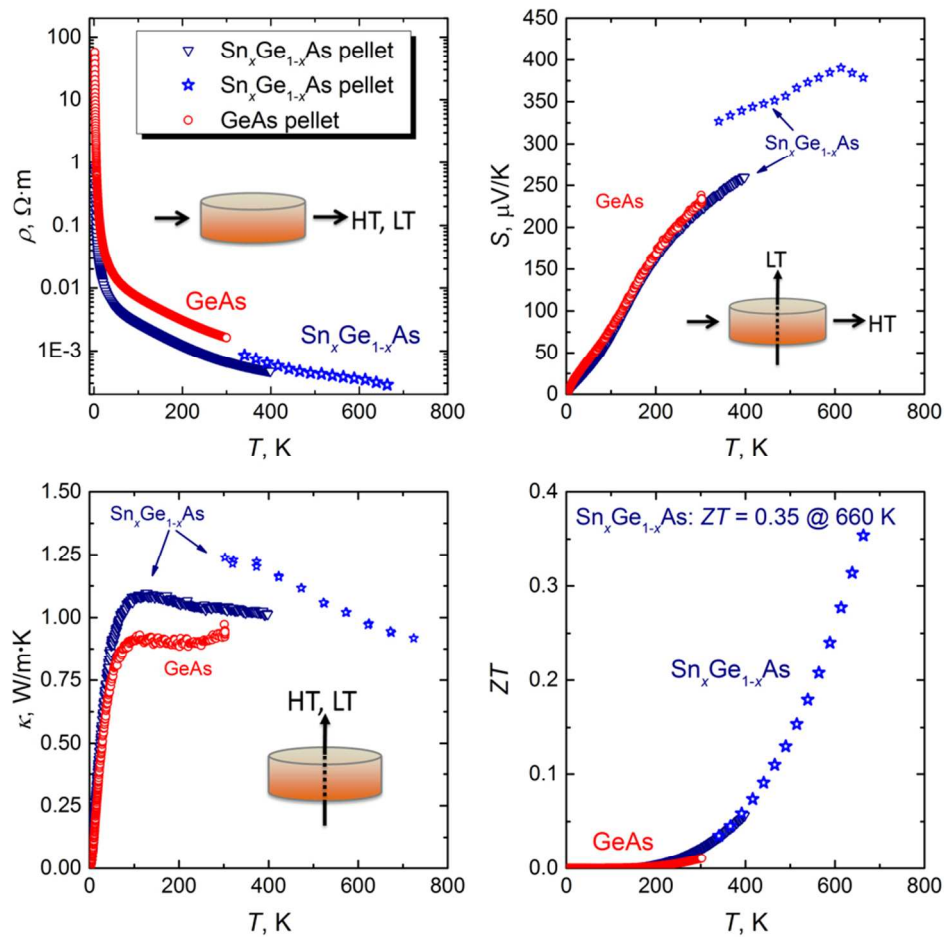
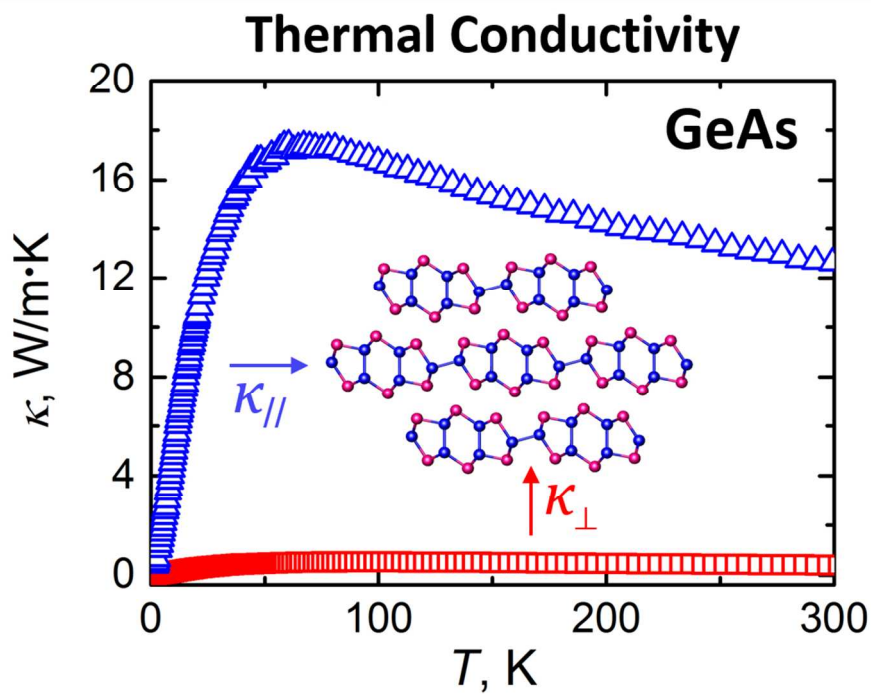


Figure 6. Resistivity, Seebeck coefficient, thermal conductivity, and figure-of-merit plots for GeAs and $\text{Sn}_x\text{Ge}_{1-x}\text{As}$ pellets. LT data are shown as circles and triangles and high temperature data are shown as blue stars.

176x175mm (150 x 150 DPI)



TOC
203x146mm (150 x 150 DPI)